The Astrophysical Journal, 806:165 (11pp), 2015 June 20 doi:10.1088/0004-637X/806/2/165

ELECTRON HEATING IN A RELATIVISTIC, WEIBEL-UNSTABLE PLASMA

Rahul Kumar, David Eichler, and Michael Gedalin
Physics Department, Ben-Gurion University, Be'er-Sheba 84105, Israel
Received 2015 January 20; accepted 2015 March 6; published 2015 June 17

ABSTRACT

The dynamics of two initially unmagnetized relativistic counter-streaming homogeneous ion–electron plasma beams are simulated in two dimensions (2D) using the particle-in-cell (PIC) method. It is shown that current filaments, which form due to the Weibel instability, develop a large-scale longitudinal electric field in the direction opposite to the current carried by the filaments as predicted by theory. This field, which is partially inductive and partially electrostatic, is identified as the main source of net electron acceleration, greatly exceeding that due to magnetic field decay at later stages. The transverse electric field, although larger than the longitudinal field, is shown to play a smaller role in heating electrons, contrary to previous claims. It is found that in one dimension, the electrons become strongly magnetized and are *not* accelerated beyond their initial kinetic energy. Rather, the heating of the electrons is enhanced by the bending and break up of the filaments, which releases electrons that would otherwise be trapped within a single filament and slow the development of the Weibel instability (i.e., the magnetic field growth) via induction as per Lenz's law. In 2D simulations, electrons are heated to about one quarter of the initial kinetic energy of ions. The magnetic energy at maximum is about 4%, decaying to less than 1% by the end of the simulation. The ions are found to gradually decelerate until the end of the simulation, by which time they retain a residual anisotropy of less than 10%.

Key words: instabilities – plasmas – relativistic processes – shock waves

1. INTRODUCTION

Collisionless shocks forming in astrophysical environments are believed to be mediated by electromagnetic instabilities (Parker 1961; Kennel & Sagdeev 1967; Eichler 1979; Blandford & Eichler 1987) in which ions are scattered by the resulting magnetic field fluctuations. In particlular, the Weibel instability (Weibel 1959), which causes fast growth of a strong magnetic field at small scales in the anisotropic plasma flow, has received much attention as the main isotropization mechanism leading to the shock transition in free-streaming ejecta from violent astrophysical events (Medvedev & Loeb 1999; Wiersma & Achterberg 2004; Lyubarsky & Eichler 2006; Achterberg & Wiersma 2007; Bret 2009; Yalinewich & Gedalin 2010; Shaisultanov et al. 2012; Shukla et al. 2012). As the dominant modes of the Weibel instability are less than the ion gyroradius, which renders them inefficient scatterers of ions, the long standing question concerning its role in collisionless shocks has been how well it competes with other mechanisms (e.g., Galeev et al. 1964; Blandford & Eichler 1987; Lyubarsky & Eichler 2006). Clearly, mechanisms that require a pre-existing magnetic field are questionable when the magnetic field is weak. On the other hand, a slow shock mechanism may actually suppress a faster mechanism because it creates a broader shock transition, and thus has greater "reach" upstream of the shock.

The role of the Weibel instability in forming the shock transition in weakly magnetized plasmas has recently been established through several numerical experiments (Nishikawa et al. 2003, 2005; Silva & Fonseca 2003; Frederiksen et al. 2004; Spitkovsky 2008; Keshet et al. 2009; Martins et al. 2009). Numerical simulations of relativistic shocks have shown that the relatively less energetic upstream electrons are significantly heated to energies comparable to the energy of ions as they cross the foreshock, which appears to be in agreement with electromagnetic observations of supernova remnants and gamma-ray burst afterglows where the high energy radiation is believed to be synchrotron radiation originating from the gyration of high-energy electrons in magnetic fields significantly higher than the interstellar magnetic field (Panaitescu & Kumar 2002; Piran 2005; Gehrels & Mészáros 2012). However, it remains unclear how the upstream electrons are energized in the foreshock region, both in nature and in the numerical simulations of collisionless shocks, and whether the Weibel instability-induced magnetic field should persist over astrophysically significant length scales behind the shock.

Numerical simulations suggest the presence of a large-scale electric field in and around the current filaments forming just ahead of the shock, and ions are found to decelerate due to this electric field. The same electric field that decelerates ions should also accelerate electrons (Blandford & Eichler 1987; Lyubarsky & Eichler 2006; Gedalin et al. 2008, 2012). However, the details of the electric field and the acceleration mechanism have not been worked out.

In order to understand the heating of electrons in the foreshock region of relativistic shocks, using the kinetic particle-in-cell (PIC) method, we simulate the development of the Weibel instability in two relativistic counter-streaming plasma beams, which resembles the precursor of a relativistic shock but is simpler and more idealized, and therefore is more suitable to resolve certain fundamental questions. The beams are taken to be homogeneous and fully interpenetrating at the beginning, so the time development of the instability in our simulation imitates the spatial development of the instability in the foreshock regions where later times in our simulation correspond the regions closer to the shock fronts. Our quantitative analysis suggests that most of the heating of upstream electrons is due to the longitudinal electric field. The transverse electric field, although much stronger than the longitudinal, has a negligible effect on the net acceleration of electrons.

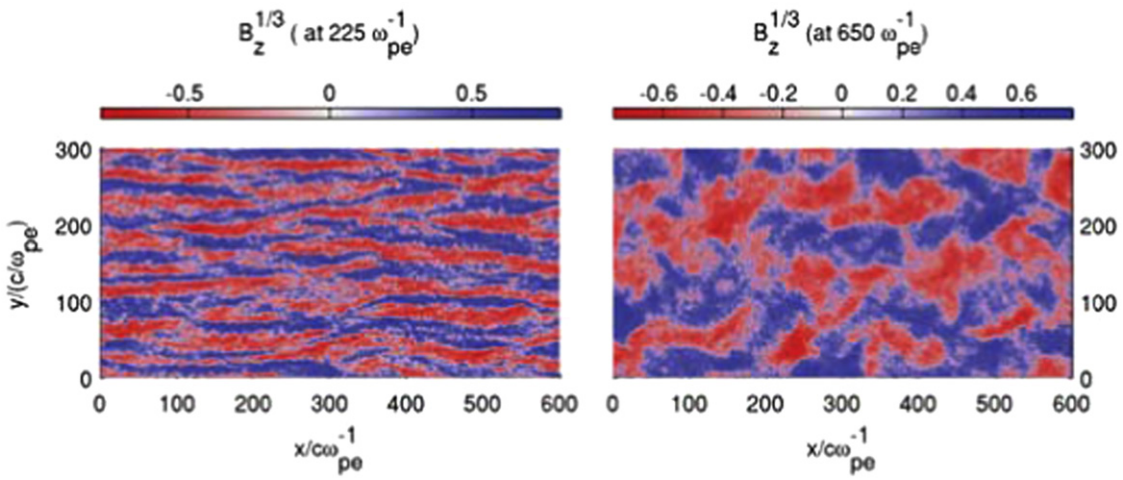

Figure 1. Left panel: structure of magnetic field at 225 ω_{pe}^{-1}. The magnetic field is still growing due to the Weibel instability and forms filamentary structures parallel to the streaming direction (referred to as filamentary phase). Most of the electron heating occurs during the filamentary phase. Right panel: structure of the magnetic field at 650 ω_{pe}^{-1}. The transverse size as well as the bending of filaments grow with time, and eventually filaments become disoriented. Henceforth, B_z and all other electromagnetic fields (i.e., E_x and E_y) are normalized to $(4\pi n_0(\gamma_0 - 1)(m_i + m_e)c^2)^{1/2}$ unless otherwise specified.

We have also inserted virtual test particles into the code to act as numerical probes. They assist in the diagnostics of the mechanisms that are at work, and this will be discussed below.

2. NUMERICAL SIMULATION

We use parallel version of the PIC code TRISTAN (Buneman 1993; Spitkovsky 2005) to simulate relativistic counter-streaming beams of ions and electrons in two dimensions (2D). The simulation is initialized by placing ion–electron pairs at uniformly chosen random locations in a 2D square box in the x–y plane. Initially, ions and electrons in each pair are moving in opposite directions along the x axis with Lorentz factor γ_0. Half of the total number of pairs have ions moving along the positive x axis while an equal number of pairs have ions moving along the negative x direction, hence creating two oppositely streaming neutral plasma beams of equal intensity where each beam has no net current. The initial condition ensures that the simulation is initially charge and current free, and that Maxwell equations are satisfied over scales where there are equal numbers of forward and backward moving electron–ion pairs; however, at the grid scale, local fluctuations in the number of forward and backward movers imply a net small-scale current. This noise level, however, is reddened by smoothening the grid scale current. As the electrons and ions in the pairs separate from each other, the electric and magnetic fields grow from the noise in the current generated by streaming electrons and ions. Since we simulate an initially unmagnetized plasma, only the out-of-plane magnetic field B_z and in-plane electric fields E_x and E_y are excited as the Weibel instability sets in. We impose periodic boundary conditions in both the x and y directions for both particles and fields.

Here, we primarily discuss results from the two largest simulations we have attempted in terms of physical size and evolution time. The ion to electron mass ratios m_i:m_e for the two reported simulations are 16:1 and 64:1, and are henceforth referred to as M_{16} and M_{64}, respectively. All of the figures in this paper represent the ion to electron mass ratio of 64:1, i.e., simulation M_{64}, unless otherwise stated. The physical sizes of the boxes for M_{16} and M_{64} are $500\ c\omega_{pe}^{-1} \times 500\ c\omega_{pe}^{-1}$ and $1000\ c\omega_{pe}^{-1} \times 1000\ c\,\omega_{pe}^{-1}$, respectively, where c is the speed of light in a vacuum and $\omega_{pe} = \sqrt{4\pi n_0 e^2/m_e\gamma_0}$ is the initial electron plasma frequency, where e is the charge of an electron and n_0 is the initial number density of electrons, or by charge neutrality, of ions. Both simulations were resolved to 1/10th of the initial electron skin-depths. There are initially 32(8) particles per unit cell of the simulation box for $M_{16}(M_{64})$ and the simulation was evolved for 500 (1000) plasma time ω_{pe}^{-1}. The ions and electrons initally move along the x axis with an initial Lorentz factor of $\gamma_0 = 10$ in the both cases.

3. FILAMENTATION AND ELECTRON HEATING

At the very beginning of the simulation, the counter-streaming electrons, which are relatively lightweight (compared to the ions) and can be relatively easily deflected by the magnetic perturbations, are subject to the Weibel instability. Current due to the streaming electrons generate a magnetic field and the electrons moving in the same direction are herded into the filaments by the self-created magnetic field. The growing current in the filaments induces an electric field opposite to the direction of the current in agreement with Lenz's law. The induced electric field slows down the streaming electrons in the filaments and are scattered by the strong magnetic field around the filaments. During this stage, relatively heavier ions continue streaming almost unaffected. As the electron Weibel instability stage ends in about $20\,\omega_{pe}^{-1}$, electrons are nearly thermalized to about their initial streaming kinetic energy $n_0 m_e(\gamma_0 - 1)c^2$, creating a nearly isotropic electron background for still streaming ions.

As the electron filamentation stage ends, relativistically counter-streaming ions undergo the Weibel instability and likewise current carrying ions are separated into long current carrying filaments along the initial streaming direction. The current filaments are non-stationary structures with slight bending in the transverse direction (Figure 1) which move along with the current carrying ions with the strength of the magnetic field being small near the filaments and large between two adjacent filaments. Again, the inductive electric field develops in the filaments opposite to the current due to the

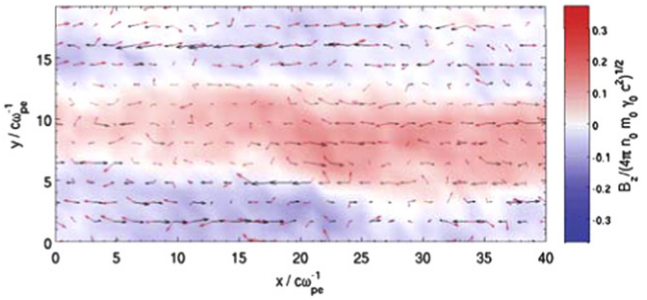

Figure 2. Local magnetic field and current due to electrons and ions are shown in a spatial patch from the simulation M_{64} (m_i:m_e = 64:1) at time 65 ω_{pe}^{-1}. The directions of the black and red arrows indicate the directions of the local current due to the ions and electrons, respectively, at the tails of the arrows, and the length of the arrow is in proportion to the magnitude of the corresponding vector quantity. The local currents shown here are computed by taking the average velocity of all particles within a box of size 0.4 $c\ \omega_{pe}^{-1} \times 0.4\ c\omega_{pe}^{-1}$ centered at the tail of arrows. The inductive electric field opposes the current due to fast moving ions in the current filaments and is responsible for the deceleration of ions as well as the acceleration of electrons.

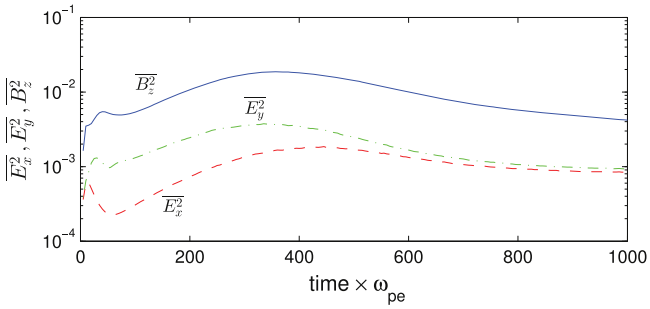

Figure 3. Temporal variations of the mean square (averaged over the physical domain of the simulation) of the electromagnetic field components E_x (dashed red), E_y (dotted–dashed green), and B_z (solid blue) are normalized to $4\pi n_0(m_i + m_e)(\gamma_0 - 1)c^2$. Among the electromagnetic fields, the magnetic field gains most of the kinetic energy lost by the ions to the fields, which holds positively charges ions in the filaments together against the electrostatic electric field, followed mostly by the electrostatic transverse electric field E_y and the longitudinal electric field E_x.

streaming ions. In addition to the inductive electric field along the filaments, an electrostatic electric field develops around the filaments transverse to the streaming direction due to an excess of positively charged ions in the filaments. The scale of this transverse electrostatic field is limited by the electrons that crowd around the filaments and remains $\sim c\omega_{pe}^{-1}$, which grows with time as the electrons are accelerated to higher energies. In Figure 2, we show the details of the local magnetic field and the local current due to ions and electrons in a small spatial part of the simulation box. The apparent correlation between the motion of ions and electrons (electrons move opposite to their current) suggests that the electrons are accelerated in the direction of the streaming ions.

The spatial distribution of electrons closely follows the distribution of ions. Charge neutralizing electrons clump in rather positively charged filaments and stream along with the ions. The electrons in the filaments move along the inductive electric field created by the streaming ions and consequently become energized. On the other hand, ions move against the electric field induced by their own current and consequently lose their energy. Since the current filaments are non-stationary and turbulent, as are the field structures, the local details of energy gain and loss for individual electrons and ions can deviate significantly from that mentioned above, and hence a statistical approach is needed to understand the systematic acceleration of electrons. We therefore compute the spatial averages of various quantities and correlations among them quantify the presence of the systemic heating of electrons at scales much larger than their skin depth.

3.1. Evolution of the Electromagnetic Fields

During the linear stage of the instability, not all the energy that is lost by the ions goes into heating the electrons. A significant part of the total kinetic energy goes into the electromagnetic fields, which are responsible for mediating the collective interactions between the charged particles. In Figure 3, we show how much of the initial kinetic energy goes into the different components of the electromagnetic fields. During the ion filamentation stage, which is mostly magnetic in nature, energy in the magnetic field reaches a few percent of the total initial kinetic energy. The longitudinal electric field E_x is the weakest component, but as we show later, is the most important for the net transfer of kinetic energy from ion to electrons. The curl of the longitudinal electric field E_x is in the direction of the magnetic field, which predominantly contributes to the growth of the magnetic field. In other words, the inductive electric field E_x accompanies the growth of the magnetic field and accelerates electrons, thus leaving it the weakest among all of the growing electromagnetic field components. As the nonlinearity sets in and the filaments are bent and broken, E_x and E_y both converge to a similar value since disruption and disorientation of current filaments wipe out any preference in the direction of the electric field in the x–y plane (Figure 1).

3.2. Electron Heating Estimate

The inductive longitudinal electric field in the direction opposite to the current in the plasma is featured in the linear theory of the Weibel instability itself. In fact, it is the curl of this longitudinal electric field which accompanies the growth of the magnetic field in agreement with Faraday's law of induction. The presence of a large-scale electric field in a conducting plasma naturally predicts the transfer of kinetic energy from ions to less energetic electrons. Here, we estimate the net energy gained by electrons due to the inductive electric field in a one dimensional (1D) linear theory of the Weibel instability. In the 2D case simulated here, electromagnetic field fluctuations due to the electrostatic wave modes parallel to the x axis (streaming direction) and the oblique modes also become comparable to the transverse modes, and eventually lead to the disruption of the current filaments (Shaisultanov et al. 2012). Here, we consider the heating of electrons solely due to transverse modes with the wave vector $\boldsymbol{k}$ along the y axis and the electric field $\boldsymbol{E}$ along the x axis. We assume homogeneity along the x axis, that is, averaging out the fluctuations along the x axis, hence reducing the problem to one spatial dimension.

Let $p_x(y)$ be the x momentum of an electron at any given location y. The electric field $E_x(y)$ at any given y determines the rate of change of x momentum for an individual electron located at y, i.e., $dp_x(y)/dt = eE_x(y)$. Averaging the x momentum of all electrons at a certain y gives

$$d\bar{p}_x(y)/dt = eE_x(y), \quad (1)$$

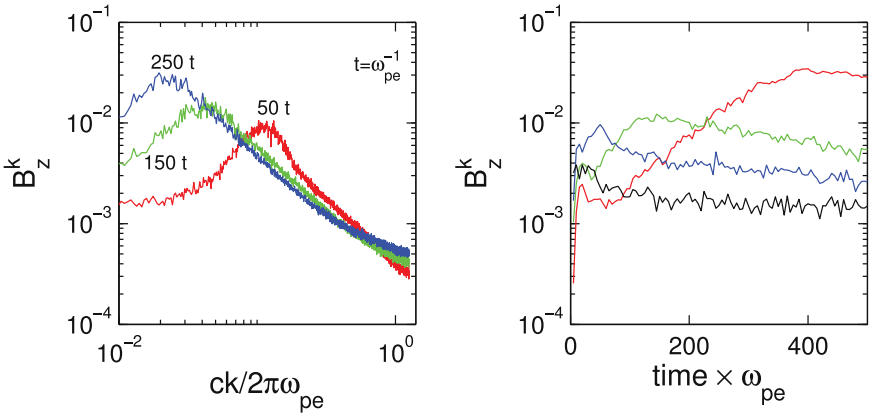

Figure 4. Left panel: average B_z^k (amplitude of magnetic field in mode of wave number k) as a function of wave number k at times 50, 150, and 250 ω_{pe}^{-1} are shown by the red, green, and blue curves, respectively. The spectrum is obtained by first computing the one dimensional discrete Fourier transform of the magnetic field in several slices of the simulation box along the transverse direction and then taking the average of the magnetic field amplitudes in any given mode k over all of these slices. Right panel: evolution of the average amplitude of the transverse magnetic fluctuations B_z^k for $2\pi/k$ = 10, 2, 1, 0.5 $c\omega_{pe}^{-1}$ are shown by red, green, blue, and black curves, respectively. The magnetic field in any given mode grows exponentially and then slowly decays.

where $\bar{p}_x(y) = \int p_x f_e(y, \boldsymbol{p}, t) d^3p \Big/ \int f_e(y, \boldsymbol{p}, t) d^3p$ with f_e being the distribution function of electrons, which is assumed to depend on y only. The electromagnetic fields E_x and B_z, as well as the mean x momentum of electrons $\bar{p}_x$, can all be written as the sum of the sinusoidal modes of various wavelengths, but with B_z one quarter a wavelength out of phase with respect to E_x and $\bar{p}_x$, since B_z is at maximum between two adjacent current filaments, whereas E_x and $\bar{p}_x$ peak in the current filaments. We first consider a single sinusoidal mode of wave number k and write $B_z = B^k \sin(ky)$, where B^k is the time-dependent amplitude of the magnetic field B_z in the mode of the wave number k. From Maxwell's equations, we relate the electric and the magnetic field as $kcE_x = \cos(ky)\partial B^k/\partial t$. Decomposing linear Equation (1) into Fourier components and then substituting for the electric field, we find

$$\partial \bar{p}_x^k / \partial t = (e/kc)\partial B^k / \partial t, \tag{2}$$

where $\bar{p}_x^k$ is the amplitude of the average x momentum $\bar{p}_x$ in the mode of the wave number k. Equation (2) enables us to express the instantaneous amplitude of an average three-momentum fluctuation in terms of the amplitude of the magnetic fluctuation as

$$\bar{p}_x^k = eB^k/kc + p_{x0}. \tag{3}$$

Equation (3) is of central importance: it implies that the gyroradius of an electron, in the limit that $p_x \gg p_{xo}$ (the momentum distribution of electrons is nearly isotropic when the ion Weibel stage starts, therefore p_{x0} is neglected hereafter), is roughly the wavelength times $1/2\pi$. As we will see below, this is confirmed by the simulations. The implication is that the field growth is *not stopped* by the magnetization of the electrons, as conjectured by Lyubarsky & Eichler (2006), because the electrons are at all times only marginally magnetized. The essential reason the electrons get heated as much as they do is that the energy of the electrons keeps pace with the field growth, and so they never become highly magnetized.

It is also shown that marginal magnetization, on the other hand, is sufficient to suppress the electron heating in 1D because the filaments remain exactly straight, and the electrons are accelerated exactly along the filaments. By contrast, in more than 1D, the existence of oblique modes allows the filaments to bend, and it becomes harder for an electron to remain within a single filament. The countercurrents of the electrons are then less likely to cancel those of the ions, and the field growth can proceed to larger length scales.

At any instant, the rate of change of the average kinetic energy of an electron $U_e = m_e(\gamma_e - 1)c^2$ due to the longitudinal electric field E_x is given by the spatial average (y-average) of $eE_x\bar{v}_x$, where $\bar{v}_x$ is p_x/m_e. For a single mode, defining U_e^k as the y average of $c\bar{p}_x^k$, we obtain (after squaring the Equation (3) and then taking the derivative with respect to time)

$$U_e^k dU_e^k / dt \approx \left[e^2c^2/(kc)^2\right] B^k \partial B^k/\partial t. \tag{4}$$

The linear theory of the Weibel instability predicts exponential growth of the amplitude of the magnetic field fluctuation B^k at all length scales. However, the maximum strength of the magnetic field at any given length scale is constrained by the available current in the plasma at that length scale. The maximum achievable net current in the filaments with a transverse size of $1/k$ is limited by the density of the streaming ions. That is to say that the maximum current in length scale $1/k$ is $\sim n_0 ec/k$, implying that $B^k_{\rm peak} \propto 1/k$ (Kato 2005; Gedalin et al. 2010). Another constraint on the peak magnetic field can be obtained from the other physical consideration that the strength of the magnetic field at any stage during instability cannot exceed the point where the current carrying ions become trapped in the current filaments (Davidson et al. 1972; Silva et al. 2002; Lyubarsky & Eichler 2006). Consequently, the growth of the magnetic field amplitude B^k at a length scale $1/k$ reaches a saturation amplitude of $B^k_{\rm peak}$, which is inversely proportional to the wave number k. The amplitude of the magnetic field B^k at smaller scales saturates first, while the magnetic field at larger scales is still growing, and the net magnetic field at any instant is dominated by the largest fully developed transverse scale. In Figure 4, we show the time evolution of the transverse spectrum of the magnetic field structure in the simulation, which confirms the exponential

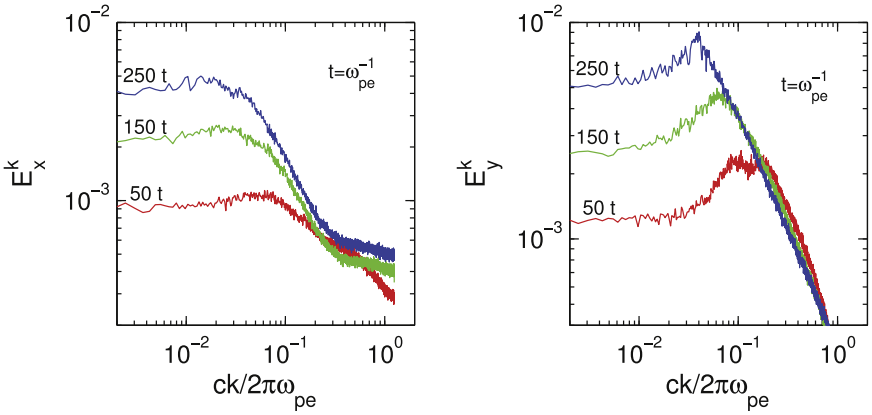

Figure 5. Transverse spectrum, as in the left panel of Figure 4, of the longitudinal electric field E_x and transverse electric field E_y as a function of wave number k at time 50, 150, and 250 ω_{pe}^{-1} are shown by red, green, and blue curves, respectively.

growth and saturation of the magnetic field at length scales smaller than a few times the skin depth of the ions. In Figure 5, we show the transverse spectrum of E_x and E_y as well. This spectrum shows the exponential growth and saturation of the transverse electric field, and that the transverse electric field peaks at half the wavelength magnetic field peaks because the transverse electric field is spatially symmetric with respect to the current filaments. The transverse spectrum of the longitudinal electric field in Figure 5 does not show saturation because of the growth of electrostatic parallel modes, as shown later, which contribute to further growth of the longitudinal electric field.

The heating due to the longitudinal electric field E_x is significant only until the filaments prevail. As the transverse scale of the filaments reach the ion skin-depth, the bending of the filaments in the transverse direction becomes significant. The current filaments start to break and become randomly oriented in the x–y plane, and the rate of heating of electrons is substantially reduced. Therefore, in order to obtain an estimate for the total energy acquired by the electrons by the end of filamentation, it is sufficient to integrate Equation (4) with respect to time for the smallest wave number $k_{\rm min}$ achieved during the Weibel instability with the electron heating in progress, and integrate it until saturation is achieved in this mode, that is, until the heating due to this mode is significant. Following these prescriptions for the net heating estimate, we get

$$U_e^{f\,2} \approx m_i \gamma_0 c^2 \left(\omega_{pi}/k_{\rm min}\, c\right)^2 \left(B_{\rm peak}^{\,k_{\rm min}\,2}/8\pi n_0\right), \qquad (5)$$

where U_e^f is the average energy of an electron toward the end of the heating process during the linear phase.

Compared to the gyro-frequency of electrons, the transverse scale of the filaments grows relatively slowly with time. Electrons gain energy in the current filaments and their Larmor radii become enlarged. However, at any instant during the linear stage of the Weibel instability, the enlarged Larmor radii of electrons due to the inductive electric field in the current filaments cannot substantially exceed the transverse size of the current filaments. This limitation of the electron Larmor radii is due to the fact that for an electron that has a Larmor radius much larger than the spacing between two adjacent filaments, the energy gained in one filament is lost in the neighboring filaments which carries the opposite current, and hence E_x is directed in the opposite sense. Additionally, as suggested by Equation (3), the energy imparted by the inductive longitudinal electric field in the largest length scale is just enough to keep the Larmor radii of the electrons at any instant at about $1/2\pi$ times the transverse size of the current filaments. As the electrons are accelerated to higher energies, their skin depth also increases in the same proportion. Indeed, as observed in the simulations (Figure 6), the ratio of the Larmor radius to the instantaneous skin depth of the electrons, which is also about $1/2\pi$ times the transverse size of the current filaments, is nearly constant during the linear stage of the Weibel instability. This suggests that during the filamentation stage the inductive heating of the electrons proceeds such that $n_0 U_e \gtrsim B^2/8\pi$ remains satisfied.

The growth of the magnetic field and the transverse size of the filaments continues until the transverse scale of the filaments becomes comparable to the ion skin depth $c\omega_{pi}^{-1}$, after which the filaments are disoriented and the heating of the electrons due to the longitudinal inductive field is substantially reduced (in the 2D case electrons continue to gain energy due to decay of magnetic field, but at a much reduced rate). This suggests that for the purpose of estimating total heating due to the inductive electric field, we can take $ck_{\rm min} \sim \omega_{pi}$. This, along with the condition that during the heating $nU_e \gtrsim B^2/8\pi$, suggest that $U_e^f \lesssim m_i \gamma_0 c^2$ (from Equation (5)), that is, the electrons are accelerated to energies comparable to the energies of ions during the linear stage of the Weibel instability due to the inductive longitudinal electric field. In the following, we present our results from the PIC simulations, which confirm that the heating of electrons due to the inductive longitudinal field is indeed significant, although there is additional heating due to the electrostatic modes in 2D simulations.

3.3. Net Work Done by the Electric Field

While the magnetic field scatters the charged particles by altering their trajectories, the only force that changes the energy of the plasma particles is generated by the electric field in the lab frame. From our PIC simulations, we separate out work done by the two orthogonal components of the electric field, namely E_x and E_y, on electrons and protons. As can be seen in Figure 8, in both of the simulations reported here, the change in the total kinetic energy of the electrons and protons is mainly due to the longitudinal electric field E_x. The net work done by

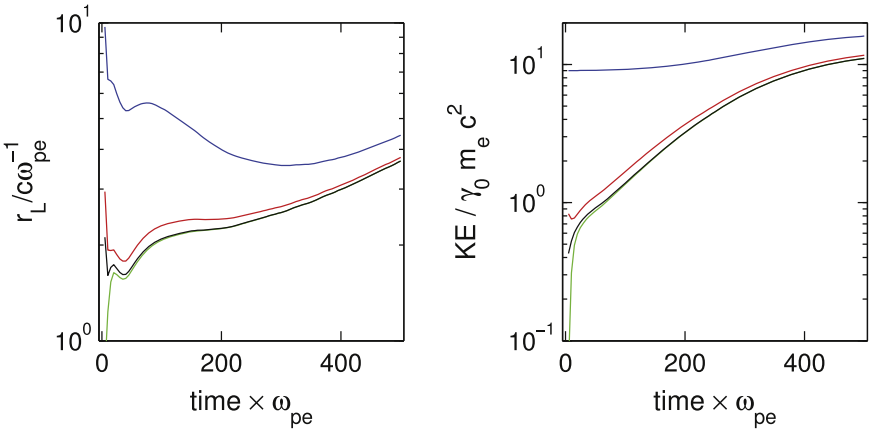

Figure 6. Left panel: the mean Larmor radii of electrons as well as test particles (charged particles that do not participate in the plasma dynamics but respond to the local electromagnetic field) with a charge to mass ratio of 0.1 of that of the electrons are shown in units of the instantaneous skin depth of electrons. The red curve shows the Larmor radius to electron skin depth ratio for electrons, while the green, black, and blue curves show the same for test particles with initial kinetic energies (isotropic mementum distribution) of 0.01, 0.1, and 10 times those of the electrons. During the linear stage of the instability, the Larmor radius of the electrons as well as of the test particles gaining energy from the longitudinal electric field remains approximately the same as the instantaneous skin depth of the electrons. Right panel: temporal variation of mean kinetic energy of the electrons and test particles in units of $\gamma_0 m_e c^2$. The color code for the curves is same as in the left panel. Energetic particles that have Lamor radii much larger than the spacing between the filaments, such as the test particles with initial kinetic energy $(\gamma_0 - 1)m_e c^2$ (shown in blue), do not become efficiently energized by the longitudinal electric field.

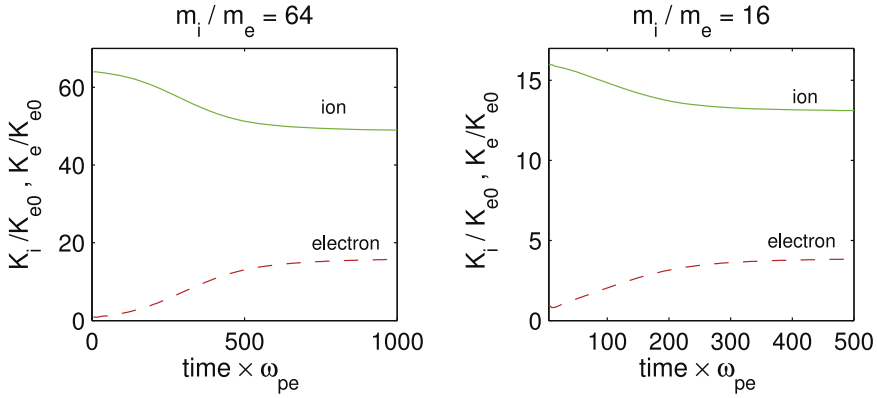

Figure 7. Evolution of the mean kinetic energy of electrons K_e (dashed red) and ions K_i (solid green) is shown for two different ion to electron mass ratios (normalized to the initial kinetic energy of electrons K_{e0}) . Electron heating due to the Lenz electric field is significant until the ion current filaments are disrupted. By the end of the simulation, the electrons are heated to about 1/3 of the ion kinetic energy in both cases considered here.

the transverse electric field E_y, which is rather stronger than the longitudinal electric field (Figure 3), is vanishingly small. The implication is that the net energization of electrons due to electrons falling into the growing and merging filaments, as suggested by Hededal et al. (2004) and Spitkovsky (2008), is rather small during the filamentation stage of the Weibel instability.

In Figure 7, we show the time evolution of the total kinetic energy of electrons and ions. It is evident from the figure that most of the energy exchange between ions and electrons takes place during the filamentation stage of the instability when the magnetic field is still growing (Figure 3) in strength. We ran the simulation long enough to capture most of the heating phase. Long after the rapid heating phase ends, electrons are found to have acquired a substantial part of the ions's kinetic energy, in agreement with the estimate presented above. Even long after the breaking of the filaments, the ions are not completely thermalized and continue to lose energy; in addition, the heating of electrons continues, though at a much lower rate.

Bending of the current filaments is apparent from the very beginning of the Weibel instability. The bending of current filaments results in a mixing of the longitudinal and transverse components of the electric field. The 2D linear theory of the Weibel instability predicts the growth of waves with a wave vector at an oblique angle with respect to the streaming direction (Shaisultanov et al. 2012), and we suggest that this can account for the bending of the filaments. The filaments are also susceptible to the Buneman instability, which leads to the growth of resonant waves parallel to the streaming direction. The oblique and parallel modes are rather electrostatic in nature (Yalinewich & Gedalin 2010; Shaisultanov et al. 2012; Stockem et al. 2014), which implies that the true nature of the longitudinal and transverse electric fields (i.e., electrostatic or induced) is rather mixed, which is due to several waves growing at the same time, although at different rates (see the Section 3.4). In order to quantify the roles of different types of growing waves in the relativistic counter-steaming plasma in the heating of electrons we separate (Helmholtz decomposition) the electric field into rotational and compressive parts, i.e., $\boldsymbol{E} = \boldsymbol{E}^c + \boldsymbol{E}^r$, such that $\nabla \cdot \boldsymbol{E}^r = 0$ and $\nabla \times \boldsymbol{E}^c = 0$. If

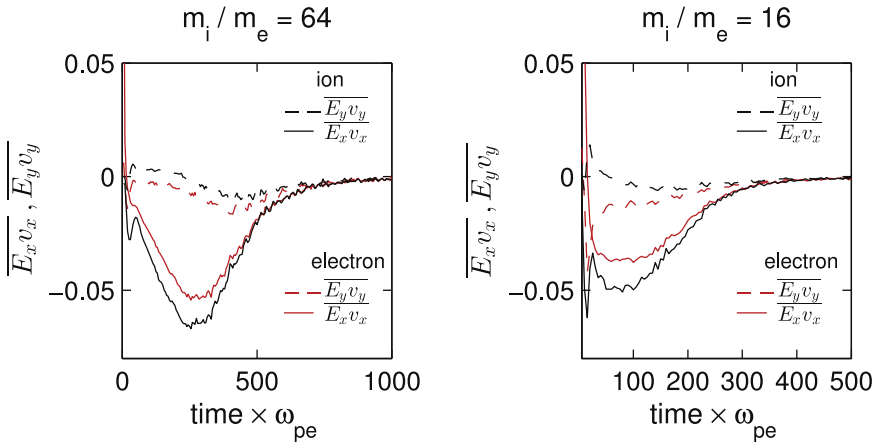

Figure 8. Rate of energy gained (lost) by electrons (protons) as a function of time due to E_x and E_y, i.e., $\overline{E_x v_x}$ and $\overline{E_y v_y}$, respectively (in units of $c^2\sqrt{4\pi\gamma_0 m_e}$), shown by solid and dashed red (black) curves, respectively . The quantities $\overline{E_x v_x}$ and $\overline{E_y v_y}$ are the mean values of $E_x v_x$ and $E_y v_y$, respectively, computed for the sample of particles (a few percent of the total number of particles) that were initially homogeneously distributed over the simulation box. The left and right panels are for the ion to electron mass ratios 16:1 and 64:1, respectively. Alhough the transverse electric field E_y is much larger in magnitude than the longitudinal electric field E_x (Figure 3), its contribution to the electron acceleration and ion deceleration (dashed lines) is negligible compared to the heating due to E_x.

the only waves growing in the counter-streaming plasma were the purely transverse Weibel modes, then the longitudinal electric field would be purely inductive in nature and could be described solely by a rotational electric field. However, in the case of oblique and parallel electrostatic waves appearing in the plasma along with the purely transverse waves, the longitudinal electric field cannot completely be described by a divergence free electric field.

In Figure 9, we show to what extent the longitudinal and transverse components of the electric field are electrostatic and inductive in nature. It is evident from the figure that during the linear stage of the instability, the transverse electric field is mostly electrostatic in nature and is caused by the excess of positive charges in the current filaments. The longitudinal electric field, on the other hand, is partially inductive and partially electrostatic, but more inductive in nature. In Figure 10, we show the work done by the rotational and compressive parts of each component of the electric field. We find that the work done by the compressive and rotational parts of the longitudinal electric field are comparable, suggesting that the role of resonant heating by electrostatic waves is comparable to the inductive heating due to transverse Weibel modes.

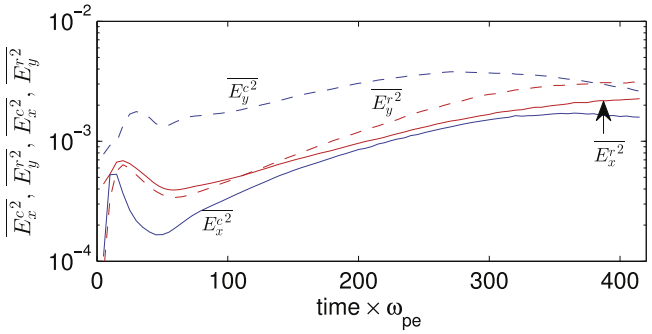

Figure 9. Temporal variation of the mean square (as in the Figure 3) of the electric field components E_x^r, E_x^c, E_y^r, and E_y^c ($\boldsymbol{E} = \boldsymbol{E}^r + \boldsymbol{E}^c$, such that $\nabla \cdot \boldsymbol{E}^r = 0$, and $\nabla \times \boldsymbol{E}^c = 0$; subscripts x and y indicate components along the longitudinal (streaming direction) and transverse directions, respectively) are shown by the solid red, solid blue, dashed red, and dashed blue curves, respectively. During the filamentation stage, the transverse electric field E_y is mostly electrostatic and the longitudinal electric field E_x is partially inductive and partially electrostatic.

3.4. Parallel and Oblique Modes

In this section, we consider the possibility that the bending of filaments is achieved by the emergence of oblique modes. Several indications of this are shown in Figures 11–14. In examining these figures, it should be kept in mind that the modes that are predominantly longitudinal (i.e., nearly parallel), $k_x \gg k_y$, have a strong electrostatic component, whereas modes that are transverse, $k_y \gg k_x$, are mostly magnetic and have relatively little electric field. The existence of oblique and nearly parallel modes can be established from Figure 11 where the longitudinal electric field E_x, has a much broader spectrum in k space than the magnetic field or the electrostatic field E_y that appears in the transverse component. Were the bending due to an instability in the longitudinal filaments themselves, one would expect that the z component of the magnetic field and the transverse electric field would develop a broadband structure (i.e., modes with sizable k_x).

To generate Figures 11–14, we performed a 2D spectral analysis of the electromagnetic field components for the simulation M_{64} to show the simultaneous growth of other waves in addition to the purely transverse Weibel waves. In Figure 12, we show the average amplitude of the sinusoidal variation in the electromagnetic fields along the streaming direction. The amplitude of variation in the magnetic field serves as a proxy for bending the current filaments since the parallel modes are mostly electrostatic and do not contribute to the growth of the magnetic field. As is evident from Figure 12, the growth of the electric field in the same length scale is faster than the growth of the magnetic field, and hence, by comparison, the rather stronger electric field in waves with wave vectors along the longitudinal direction can be attributed to the growth of electrostatic modes along the streaming direction in addition to the contribution from the bending of current filaments.

In Figure 14, we show the growth of the magnetic and electric fields in purely transverse, purely longitudinal, and

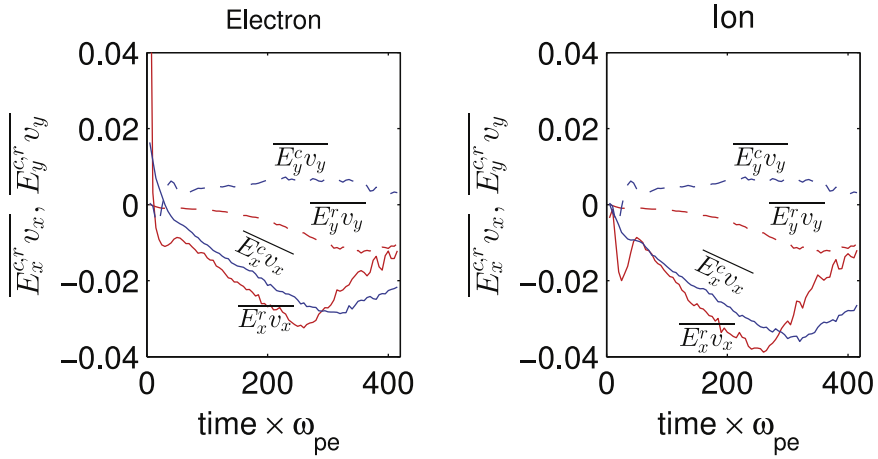

Figure 10. Left (right) panel shows the instantaneous rate of energy gained (lost) by the electrons (protons) due to the rotational and compressive components of the longitudinal electric field in solid red and solid blue, respectively. The dashed red and blue curves shows the same due to the rotational and compressive components of the transverse electric field E_y, respectively. Normalization and computation of the mean shown here are the same as in the Figure 8.

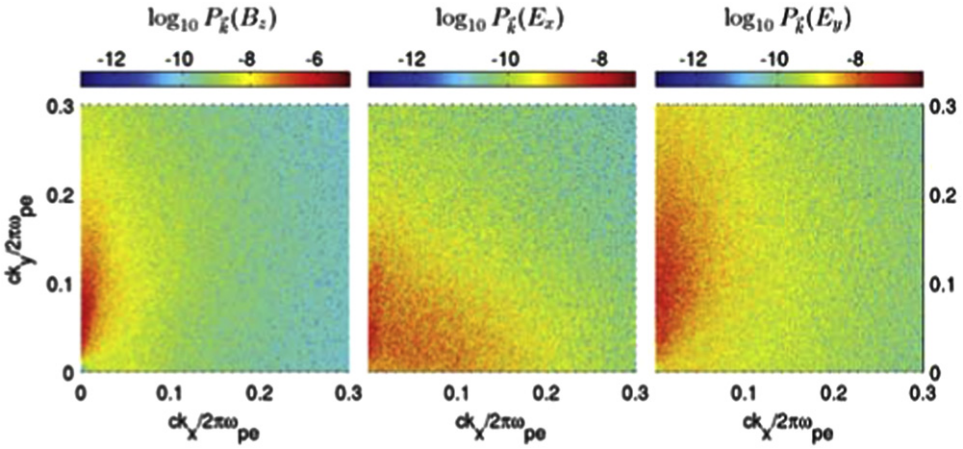

Figure 11. Power spectrum for B_z, E_x, and E_y at 100 ω_{pe}^{-1} is shown in the left, middle, and right panels, respectively. The power spectrum shows the broadband nature of the Weibel instability. The spectrum of B_z shows that the transverse waves are mostly magnetic in nature. The existence of parallel and oblique modes, which are rather electrostatic in nature, is apparent from the spectrum of E_x. At this time, about 10% of the total wave energy is in the fastest growing mode—the purely transverse one. The other 90% resides in other modes, of which there are many more.

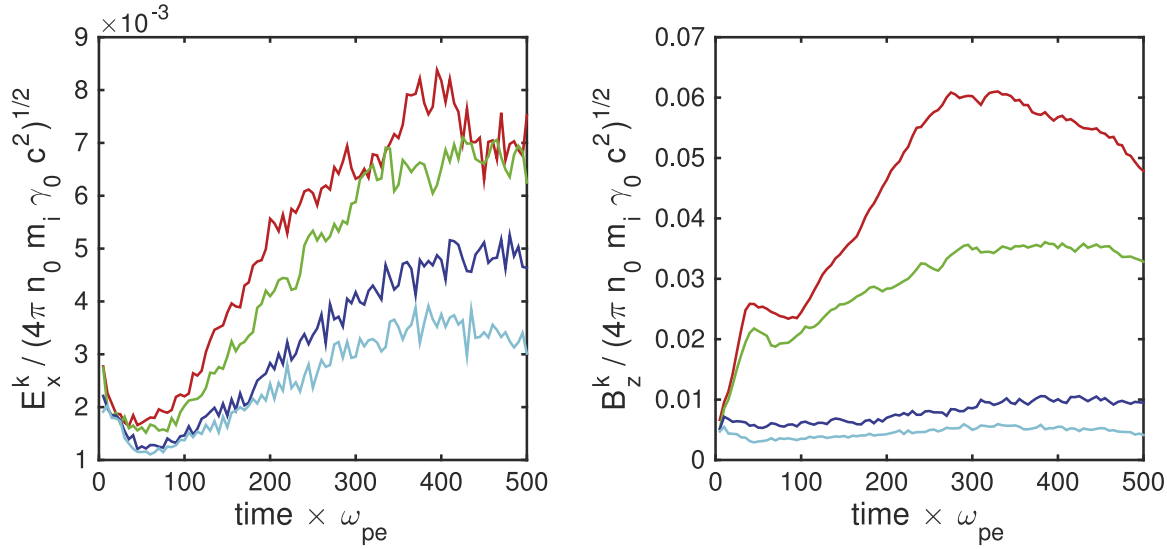

Figure 12. Left (right) panel shows the temporal evolution of the average amplitude of sinusoidal variation in the longitudinal electric (magnetic) field E_x^k (B_z^k) with the wave vector along the streaming direction (x axis). The red, green, blue, and cyan curves show the field amplitude of modes with $2\pi/k = 410$, 90, 16, and 8 $c\omega_{pe}^{-1}$, respectively. The average amplitudes shown here are obtained after taking the average of the amplitude of any given mode over an ensemble of several slices parallel to the y axis at equally spaced locations along the x axis.

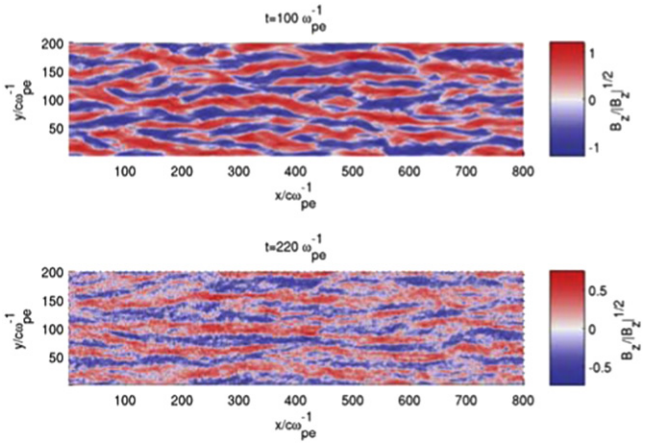

Figure 13. Strength and sense of the magnetic field shown in a small patch of the simulation box for two variations of simulations M_{64} when the transverse size of the filaments is approxiamtely 30 $c\omega_{pe}^{-1}$. Top panel: only counter-streaming ion beams (immobile or infinite mass electrons are assumed to be sitting at the initial locations of ions in order to achieve charge neutrality). Bottom panel: simulation M_{64} in which electrons are also participating in the plasma dynamics. All modes grow faster in the absence of electrons which resonantly suppress the growth of waves.

oblique modes. The general trend is that the purely transverse modes grow fastest and the rate of growth decreases with the angle between the wave vector and the y axis. The oblique modes, like the purely transverse mode, are suppressed in the linear regime by the inductive response of the electrons which are accelerated by, and therefore move along, the inductive electric fields. Note, however, that the purely transverse mode stops growing at time of about 250 ω_{pe} (Figure 14) while the oblique modes continus to grow, and in fact catch up with the purely transverse mode. This can be interpreted as follows: the transverse mode, as the fastest growing, is the first to trap the electrons into resonance, and so the number of resonant electrons actually increases. This includes those electrons that resonated with the oblique modes until trapped by the purely transverse mode. We can say that these electrons are in a nonlinear resonance with the purely trapped mode. At this point, the growth of the purely transverse mode is impeded by the even larger number of nonlinearly resonant electrons, and so it stops growing. The oblique modes, in contrast, suffer less from the inductive effects of the electrons and keep growing until they have spoiled the alignment of the filaments made by the purely transverse mode.

The role of electrons in suppressing the oblique modes can clearly be demonstrated by simulating the Weibel instability with electrons of infinite mass such that electrons do not interact with the plasma waves. In the absence of lighter resonating electrons, all modes grow faster and the Weibel instability gives rise to a rather strong magnetic field (Figure 13). In the case of infinitely massive electrons, the current filaments which form due to the Weibel instability are rather short in length along the longitudinal direction and quickly become disoriented compared to the simulation with electrons interacting with the waves.

The large fluctuations in the amplitudes of the waves (Figure 14) are apparently due to the interference of waves with same wave number but with different phases appearing in the plasma at different spatial locations which grow independently. The phase difference in the purely transverse Weibel modes at different locations can also contribute to the wiggle in the filaments which appears at the very beginning of the simulation and can contribute to the scattering of the electrons.

The power spectrum of the electromagnetic fields (Figure 11) reveals the broadband nature of the instabilities in the counter-streaming plasma. In our simulation, we have identified the growth of transverse and oblique Weibel-like modes as well as parallel electrostatic modes. However, there may be several other waves and instabilities in the counter-streaming plasma (Bret 2009) which make the current filaments unstable, and may become more pronounced for plasma parameters that are rather more realistic for astrophysical contexts, i.e., for a higher ion to electrons mass ratio or a larger Lorentz factor of the streaming plasma. In any case, it is evident that whichever wave can bend the current filaments of streaming ions can very efficiently scatter electrons out of the filaments since the electrons have much less inertial mass compared with ions. The bending of the filaments, which we suggest is due to the broadband nature of the Weibel instability (i.e., growth of the waves with their wave vector at some angle with respect to the transverse direction), is a crucial requirement for the heating of the electrons as demonstrated by the 1D simulation where poor scattering results in trapped electrons, which efficiently short out the inductive electric field created by streaming ions and do not become energized.

3.5. 1D Simulation: Purely Transverse Weibel Mode

In order to illustrate the role of the oblique and electrostatic modes parallel to the streaming direction, we simulated the counter-streaming plasma in 1D such that the only modes transverse to the streaming direction, i.e., the purely transverse Weibel models, are allowed to grow. The growth of oblique as well as longitudinal modes is suppressed by reducing the size of the box along the streaming direction (x axis) to the sub-skin depth level, and hence reducing the simulation to effectively 1.5 dimensions. That is to say, though the electromagnetic field and particle velocity are allowed to have all three components, they are only allowed to vary along the transverse direction (y axis). Here, we discuss the results from a simulation which has a 2D box of size $0.3 \times 1600\ c\omega_{pe}^{-1}$ and 64 particles per cell. All other parameters for this simulation are the same as in the case of the 2D simulation M_{64}.

In the 1D simulation, electrons first undergo the Weibel instability, which is essentially the Weibel instability of one species. The electron Weibel stage ends with the isotropization of electrons. As the ions undergo the Webiel instability, the size of the ion current filaments and the strength of the magnetic field grow. At the stage where the transverse size of the current filaments becomes $\sim 2\pi c\omega_{pe}^{-1}$, electrons, which are magnetized, are confined in ion current filaments between two adjacent peaks of the magnetic field (Wiersma & Achterberg 2004; Lyubarsky & Eichler 2006). Electrons in the current filaments quiver in the transverse direction and drift in the same sense as the ions. The countercurrent due to the electrons efficiently arrests the growth of the Weibel instability of the ions. Anisotropic ions continue to stream in the current filaments and the growth of the magnetic field ceases (Figure 15). The lack of heating of electrons observed in the 1D case can be attributed to the lack of scattering of electrons out of the current filaments which is rather efficient in the 2D case due to the oblique waves growing along with the purely transverse mode.

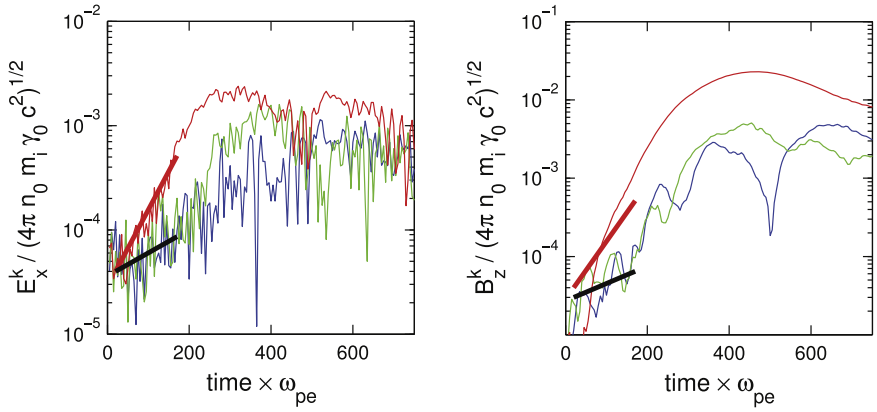

Figure 14. Left (right) panel shows the temporal evolution of the amplitude of the sinusoidal variation (obtained from a two-dimensional Fourier spectrum of the electromagnetic fields) in the longitudinal electric (magnetic) field E_x^k (B_z^k) with the wave vector along the x axis, y axis, and at an equal angle with respect to the x and y axes. Specifically, the red, green, and blue curves correspond to $(2\pi/k_x, 2\pi/k_y) = (\infty, 100)$, $(100, 100)$, and $(100, \infty)$ $c\omega_{pe}^{-1}$, respectively. The thick solid line segments in red and black indicate the growth rate predicted by the linear theory (taken from Shaisultanov et al. 2012 for the electron temperature m_e/m_i times the ion temperature) for the transverse and oblique waves, respectively.

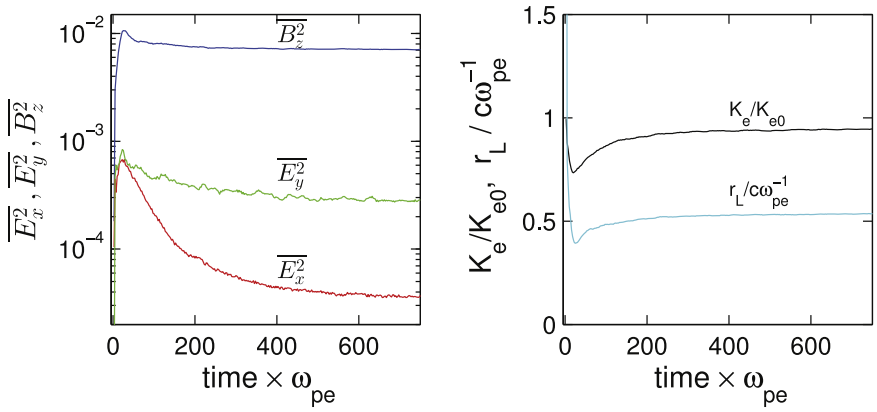

Figure 15. 1D simulation: (A) Left panel: the temporal variation of the mean square (averaged over the physical domain of the simulation) of the electromagnetic field components E_x (red), E_y (green), and B_z (blue) are normalized to the total initial kinetic energy density $n(m_i + m_e)(\gamma_0 - 1)c^2$. (B) Right panel: (a) Black curve: temporal variation of the kinetic energy of electron K_e (normalized to the initial kinetic energy of electrons $K_{e0} = (\gamma_0 - 1)m_e c^2$), (b) Cyan curve: ratio of the instantaneous Larmor radius to the instantaneous skin depth of electrons as in Figure 6.

4. DISCUSSION AND CONCLUSIONS

We have simulated the development of the Weibel instability in relativistically counter-streaming homogenous ion–electron beams using the kinematic PIC method. The physical domain of the simulation is taken to be sufficiently large, both parallel and perpendicular to the plasma streaming direction, to ensure that the growth of the Weibel-unstable modes as well as the longitudinal electrostatic states are not frustrated due to the finite size of the box. The homogeneous set-up simulated here ensures that any effect of large-scale longitudinal inhomogeneity which may be present in the case of the shock is separated out. In the case of a shock transition, there might be some additional heating due to the cross-shock potential which may develop because of the longitudinal separation of ions from electrons, since the lighter electrons can be relatively easily isotropized by the foreshock magnetic field, hence interrupting the electron flow before the flow of ions (Balikhin et al. 1993; Lyubarsky 2006; Lyubarsky & Eichler 2006; Gedalin et al. 2008).

Our findings from the plasma simulations concerning the heating of electrons can be summarized as follows.

1. In the case of the relativistic counter-streaming homogeneous plasma beams, except in 1D, electrons are accelerated to an energy comparable to the energy of ions and most of the heating occurs during the formation and bending of the filaments and little after the filaments disrupt and disorient.
2. A comparison of the net work done by the longitudinal and transverse electric fields shows that the main force that takes energy away from the ions and accelerates electrons is due to the longitudinal electric field.
3. The work done by the transverse electric field is negligibly small compared to the longitudinal electric field and increasingly so for larger ion to electron mass ratios (Figure 8).
4. Decomposition of the electric field into electrostatic and inductive components reveals that the longitudinal components is partially inductive, which is due to the growing current in the current filaments, and partially electrostatic, which is due to the bending of the current filaments and the growth of electrostatic waves along the longitudinal direction. The transverse component, on the

other hand, is mainly electrostatic in nature and is due to the separation of charges.

5. Calculation of the rate of net work done on the electrons and ions by the electrostatic and inductive components of the longitudinal electric field shows that the work done by both components are comparable, with that of the inductive component being slightly larger. This suggests that part of the acceleration of electrons is due to the fast moving chunks of current filaments (fermi-like heating, presumably second order).
6. We showed that background electrons efficiently take energy away from the waves generated by the unstable counter-streaming ions, and hence significantly alter the dynamics of the instabilities in the counter-streaming plasma. It then becomes essential to take continuous energization of the electrons into account in order to calculate the growth of various wave modes, even in the linear approximations.
7. The 2D power spectrum of the electromagnetic fields reveals the broadband nature of the instabilities in the counter-streaming plasma (Figure 11). In particular, it shows the existence of the oblique and parallel modes, of which the oblique modes is suggested to be primarily responsible for bending and the eventual break up of the current filaments.
8. The Fourier spectrum of the electromagnetic fields suggests that waves of the same wave number but with different phases develop in the simulation and that there is significant phase mixing which can partially be responsible for the instability of filaments and the scattering of electrons.

Current filamentation and significant electron heating is observed in three-dimensional simulations of counter-steaming plasma as well. We expect that the physical mechanisms in a more realistic 3D simulation should be the same as in the 2D case discussed here and can be verified in future simulations.

We thank U. Keshet, Y. Lyubarsky, and A. Spitkovsky for helpful discussions. We thank A. Spitkovsky for a critical reading of the manuscript. We are grateful to U. Keshet for kindly providing us with computational resources for the simulations. R.K. and D.E. acknowledge support from the Israel-U.S. Binational Science Foundation and the Israeli Science Foundation. M.G. was partially supported by the Israel Science Foundation (grant No. 368/14).

REFERENCES

Achterberg, A., & Wiersma, J. 2007, A&A, 475, 1
Balikhin, M., Gedalin, M., & Petrukovich, A. 1993, PhRvL, 70, 1259
Blandford, R., & Eichler, D. 1987, PhR, 154, 1
Bret, A. 2009, ApJ, 699, 990
Buneman, O. 1993, in Computer Space Plasma Physics: Simulation Techniques and Software, ed. H. Matsumoto, & Y. Omura (Terra Scientific: Tokyo)
Davidson, R. C., Hammer, D. A., Haber, I., & Wagner, C. E. 1972, PhFl, 15, 317
Eichler, D. 1979, ApJ, 229, 419
Frederiksen, J. T., Hededal, C. B., Haugblle, T., & Nordlund 2004, ApJL, 608, L13
Galeev, A. A., Moiseev, S. S., & Sagdeev, R. Z. 1964, JNuE, 6, 645
Gedalin, M., Balikhin, M. A., & Eichler, D. 2008, PhRvE, 77, 026403
Gedalin, M., Medvedev, M., Spitkovsky, A., et al. 2010, PhPl, 17, 032108
Gedalin, M., Smolik, E., Spitkovsky, A., & Balikhin, M. 2012, EL, 97, 35002
Gehrels, N., & Mészáros, P. 2012, Sci, 337, 932
Hededal, C. B., Haugblle, T., Frederiksen, J. T., & Nordlund, Ã. 2004, ApJL, 617, L107
Kato, T. N. 2005, PhPl, 12, 080705
Kennel, C. F., & Sagdeev, R. Z. 1967, JGR, 72, 3303
Keshet, U., Katz, B., Spitkovsky, A., & Waxman, E. 2009, ApJL, 693, L127
Lyubarsky, Y., & Eichler, D. 2006, ApJ, 647, 1250
Lyubarsky, Y. 2006, ApJ, 652, 1297
Martins, S. F., Fonseca, R. A., Silva, L. O., & Mori, W. B. 2009, ApJL, 695, L189
Medvedev, M. V., & Loeb, A. 1999, ApJ, 526, 697
Nishikawa, K.-I., Hardee, P., Richardson, G., et al. 2003, ApJ, 595, 555
Nishikawa, K.-I., Hardee, P., Richardson, G., et al. 2005, ApJ, 622, 927
Panaitescu, A., & Kumar, P. 2002, ApJ, 571, 779
Parker, E. N. 1961, JNuE, 2, 146
Piran, T. 2005, RvMP, 76, 1143
Shaisultanov, R., Lyubarsky, Y., & Eichler, D. 2012, ApJ, 744, 182
Shukla, N., Stockem, A., Fiuza, F., & Silva, L. O. 2012, JPlPh, 78, 181
Silva, L. O., Fonseca, R. A., Tonge, J. W., Mori, W. B., & Dawson, J. M. 2002, PhPl, 9, 2458
Silva, L. O., Fonseca, R. A., Tonge, J. W., et al. 2003, ApJL, 596, L121
Spitkovsky, A. 2005, in American Institute of Physics Conf. Ser. 801, Astrophysical Sources of High Energy Particles and Radiation, ed. T. Bulik, B. Rudak, & G. Madejski (New York: AIP), 345
Spitkovsky, A. 2008, ApJL, 673, L39
Spitkovsky, A. 2008, ApJL, 682, L5
Stockem, A., Fiuza, F., Bret, A., Fonseca, R. A., & Silva, L. O. 2014, NatSR, 4, 3934
Weibel, E. S. 1959, PhRvL, 2, 83
Wiersma, J., & Achterberg, A. 2004, A&A, 428, 365
Yalinewich, A., & Gedalin, M. 2010, PhPl, 17, 062101